MATERIALS CHEMISTRY FRONTIERS

RESEARCH ARTICLE

View Article Online
View Journal | View Issue

Cite this: *Mater. Chem. Front.*, 2026, **10**, 80

Carbohydrate-powered solar cells: how starches give perovskite extra energy

Chinnatip Harnmanasvate,[a] Rico Meitzner,[b] Yuxin Liu,[c] Nopporn Rujisamphan,[d] Eva Unger[bc] and Rongrong Cheacharoen *[ae]

Perovskite solar cells (PSCs) have emerged as promising low-cost photovoltaics, combining high efficiency with solution-processable and scalable fabrication. Realizing stable PSCs *via* ambient-condition processing is critical for practical, large-area manufacturing. Natural additives offer a sustainable means to direct perovskite crystallization and improve film quality; however, the relationship between their molecular structure and perovskite nucleation, defect passivation, and stability—especially under high-humidity conditions—remains underexplored. Here, we systematically investigate the impact of starch structures, focusing on the ratio of linear amylose to branched amylopectin, on perovskite formation at 50% relative humidity. We demonstrate that amylose-rich starch templates the growth of highly oriented, compact perovskite films with significantly suppressed defect densities. This molecular templating enhances the optoelectronic quality of the perovskite absorber, resulting in a 15% improvement in the power conversion efficiency of all-solution-processed carbon-based PSCs. Moreover, devices incorporating amylose exhibit markedly improved operational stability, with suppressed burn-in and a doubled T_{80} lifetime under ISOS-L-1 testing. These results reveal the crucial role of natural polymer structures in modulating crystallization pathways and defect chemistry under real-world conditions. Our findings establish a design principle for sustainable, ambient condition-processable PSC fabrication and provide a blueprint for eco-friendly additive engineering in hybrid optoelectronic materials.

Received 11th July 2025,
Accepted 12th November 2025

DOI: 10.1039/d5qm00493d

rsc.li/frontiers-materials

1. Introduction

Hybrid metal–halide perovskite solar cells (PSCs) have emerged as a next-generation energy technology to supply the escalating global energy demand.[1] However, the fabrication of most high-efficiency PSCs still relies on expensive environmental control chambers and vacuum systems, which are huge barriers for scaling-up and commercializing PSCs.[2,3] Minimizing the usage of complex and energy-intensive processes by enabling fabrication in an ambient environment with some level of humidity and employing solution-processable carbon top-electrodes offer pathways to scalable and cost-effective PSC production.[4] Nonetheless, depositing high-quality perovskite films in ambient air is challenging due to the sensitivity of perovskite materials to moisture, resulting in defective perovskite films.[5] This issue can accelerate ion migration and non-radiative recombination, which limit the efficiency and stability of PSCs.[1,6] Therefore, optimizing perovskite inks by incorporating additives that modulate the formation of high-quality PSK layers under ambient conditions—regardless of fluctuation in humidity levels—is of high interest.

Additive engineering of perovskite precursors is a cost-efficient and less-complex strategy for achieving high-quality perovskite absorbers under ambient conditions.[7,8] Various materials, for example, organic molecules, ionic liquids, salts, polymers, *etc.*,[9,10] have been introduced as additives to regulate the formation process of perovskite in ambient air by mitigating perovskite-moisture interactions, thereby enhancing perovskite film morphology.[11–13] However, small-molecule additives (*i.e.*, organic molecules, liquid ions, and salts) exhibit a high diffusion coefficient and volatility degree, which could affect the stability of PSCs under real-world operating conditions.[14,15] Therefore, polymeric materials present a compelling alternative as additives, offering the dual functionality of templating perovskite growth and forming stable immobilized networks at grain boundaries. This dual role not only enhances the film quality but also helps mitigate the pathway of environmental-induced degradation.[16] Nonetheless,

[a] *International Graduate Program in Nanoscience & Technology, Graduate School, Chulalongkorn University, 10330, Bangkok, Thailand. E-mail: Rongrong.C@chula.ac.th*
[b] *Helmholtz-Zentrum Berlin für Materialien und Energie GmbH, 14109, Berlin, Germany*
[c] *Institut für Chemie & IRIS Adlershof Humboldt-Universität zu Berlin, 12489, Berlin, Germany*
[d] *Nanoscience and Nanotechnology Graduate Program, Faculty of Science, King Mongkut's University of Technology Thonburi, 10140, Bangkok, Thailand*
[e] *Metallurgy and Materials Science Research Institute, Chulalongkorn University, 10330, Bangkok, Thailand*

most polymer additives are derived from petrochemical sources, raising environmental concerns like ecosystem disruption, pollution, and high carbon emissions. In contrast, natural polymers offer lower cost, less toxicity,[17] and nearly nine times smaller carbon footprint,[18,19] positioning them as attractive candidates for PSC fabrication under ambient conditions.

Natural polymers—such as polysaccharides, polypeptides, and polynucleotides—are promising green additives for perovskite precursors due to their long covalent chains with enriched functional groups such as hydroxyl (–OH), amino ($–NH_2$), and carboxyl (–COOH), which are beneficial for crystal growth and defect passivation.[20–22] Additionally, these natural materials exhibit diverse molecular structures, such as linear and branched structures, which could influence the formation kinetics of perovskite.[23] So far, there has been a lack of studies on the structure–property relationships of natural polymers with regard to linear or branching structures; we therefore decided to use starches with different contents of amylose (a linear-helical chain) and amylopectin (a helical chain with branching)[24] as a vehicle to study these relationships. Starches also contain numerous hydroxyl (–OH) groups[24] along their polymeric chains, which are advantageous for templating the perovskite growth and defect passivation.[13,25] Despite their chemical functionalities, the application of starch-based additives in high-humidity perovskite processing has not been widely studied, presenting an opportunity to enhance the sustainability of PSC production under ambient conditions.

In this study, we investigate how the structure of polysaccharides influences perovskite growth under a tropical climate with high humidity and high temperature (50 ± 10%RH, 30 ± 5 °C) by comparing two Thai starches: sticky rice (completely branched amylopectin) and mung bean (a roughly equal mixture of linear amylose and amylopectin). For the first time, we unveil the impact of amylose, a linear polysaccharide, on the perovskite formation pathway by a combination of *in situ* photoluminescence (*in situ* PL) and Fourier-transform infrared spectroscopy (FTIR). Moreover, we observe the impact of perovskite growth assisted by linear amylose on the quality of perovskite absorbers by scanning electron microscopy (SEM) together with X-ray diffraction (XRD). To further explore the influence of amylose on the optoelectronic properties of perovskite thin films, we conduct space-charge-limited current (SCLC) and PL spectroscopy. Lastly, we investigate the effect of starch modification on the performance and operational stability (ISOS-L1) of fully solution-processed carbon-based solar cells.

2. Experimental section

2.1 Materials

Formamidinium iodide (>99.99%, FAI) and lead(II) iodide (99.99%, PbI_2) were purchased from GreatCell and TCI, respectively. Lead(II) bromide (>98%, $PbBr_2$), cesium iodide (99.999%, CsI), lithium bis(trifluoromethanesulfonyl)imide (99.99%, Li–TSFI), nickel nitrate hexahydrate (>98.5%), ethylenediamine (>99.5%), ethylene glycol (anhydrous >99.8%), chlorobenzene (anhydrous >99.8%, CB), *N*,*N*-dimethylformamide (anhydrous 99.8%, DMF), and dimethyl sulfoxide (anhydrous >99.9%, DMSO) were obtained from Sigma-Aldrich. *N*2,*N*2,*N*2′,*N*2′,*N*7,*N*7,*N*7′,*N*7′-Octakis(4-methoxyphenyl)-9,9′-spirobi[9*H*-fluorene]-2,2′,7,7′-tetramine (99.86%, Spiro-OMeTAD) and [6,6]-phenyl-C61-butyric acid methyl ester (PCBM) were supplied by Advance Election Technology. Colloidal-SnO_2 (15 wt% in H_2O), 4-*tert*-butylpyridine (>98%, 4-tBP) and acetonitrile (>99.5% (GC), AceN) were provided by Alfa-Aesar, Advance Election Technology, Ossila and TCI, respectively. Sticky-rice and mung bean starch additives were purchased from Thai local companies, Bangkok Inter Food Co., Ltd and Sitthinan Co., Ltd, respectively.

2.2 Solution preparation

A 15 wt% colloidal-SnO_2 solution was diluted in de-ionized water down to 3.75 wt% and then sonicated for 1 h in an ultrasonic bath. 1.5 M $Cs_{0.17}FA_{0.83}Pb(I_{0.83}Br_{0.17})_3$ (CsFA) perovskite precursor was prepared by dissolving FAI, CsI, $PbBr_2$ and PbI_2 powders in DMF : DMSO with a ratio of 4 : 1. Additionally, starches, including, sticky rice and mung bean starches, were added to the perovskite precursor at an optimized 0.25 mg mL^{-1} concentration, as shown in Fig. S1, by stirring at 70 °C for 3 h. Before the perovskite deposition process, all precursors were filtered through a 0.22 μm polytetrafluoroethylene (PTFE) filter. Nickel nitrate hexahydrate was dissolved in ethylenediamine and ethylene glycol at 1 M concentration, and then filtered through a 0.22 μm PTFE filter.[26] The Spiro-OMeTAD solution was prepared following our previous work.[27] PCBM solution was prepared by dissolving PCBM powder in chlorobenzene at 20 mg mL^{-1} concentration. Perovskite, Spiro-OMeTAD, nickel oxide and PCBM solutions were prepared in a nitrogen-filled glovebox.

2.3 Perovskite solar cell fabrication process

FTO-coated glass substrates were sequentially cleaned using Alconox, DI water, acetone and isopropanol by ultrasonication for 15 min. Afterward, the substrates were cleaned by UV-O_3 treatment for 15 min. Then, 100 μL of the colloidal-SnO_2 solution was dropped on a UV-O_3 treated substrate at 3000 rpm for 30 s, and this step was repeated before annealing at 150 °C for 1 h. Then, the SnO_2-coated substrates were treated with UV-O_3 for 15 mins. Subsequently, 50 μL of the perovskite precursors were dropped on the substrates, then spun at 1000 rpm for 14 s before ramping up to 6000 rpm for 10 s. During the second spinning process, N_2 gas, which was set at 6 bar pressure, was blown on the wet perovskite film at 1.5 cm height and then immediately moved to anneal on a 150 °C hot-plate for 10 min. Next, the substrates were transferred to a nitrogen-filled glovebox (<0.1 ppm H_2O, <0.1 ppm O_2) for hole transport layer (HTL) deposition. For conventional devices, 40 μL of the Spiro-OMeTAD layer was dropped on the perovskite films, then spun cast at 3000 rpm for 20 s. After HTL deposition, all substrates were stored overnight under a <10%RH atmosphere. A carbon electrode was prepared by blading commercial carbon paste on graphite foil with 80 μm thickness before soaking in ethanol for 2 h. Afterward, the electrode was pressed

on the devices with 0.6 MPa and at 50 °C for 180 s. The SnO_2, perovskite and electrode layers were deposited and processed in ambient air at 50 ± 10% RH and 30 ± 5 °C.

2.4 Electron and hole only device preparation

FTO substrates were cleaned and prepared following the steps in the perovskite solar cell fabrication process. For an electron only device, colloidal-SnO_2 was coated on the FTO substrate before depositing the perovskite layer. Then, PCBM was deposited on the perovskite layer by spin-coating at 1000 rpm for 30 s[28] before storage in a <10%RH desiccator overnight. For a hole only device, NiO_x was deposited on the FTO substrates following the previous work;[29] then, the perovskite layer was deposited. Consequently, Spiro-OMeTAD was coated on top of

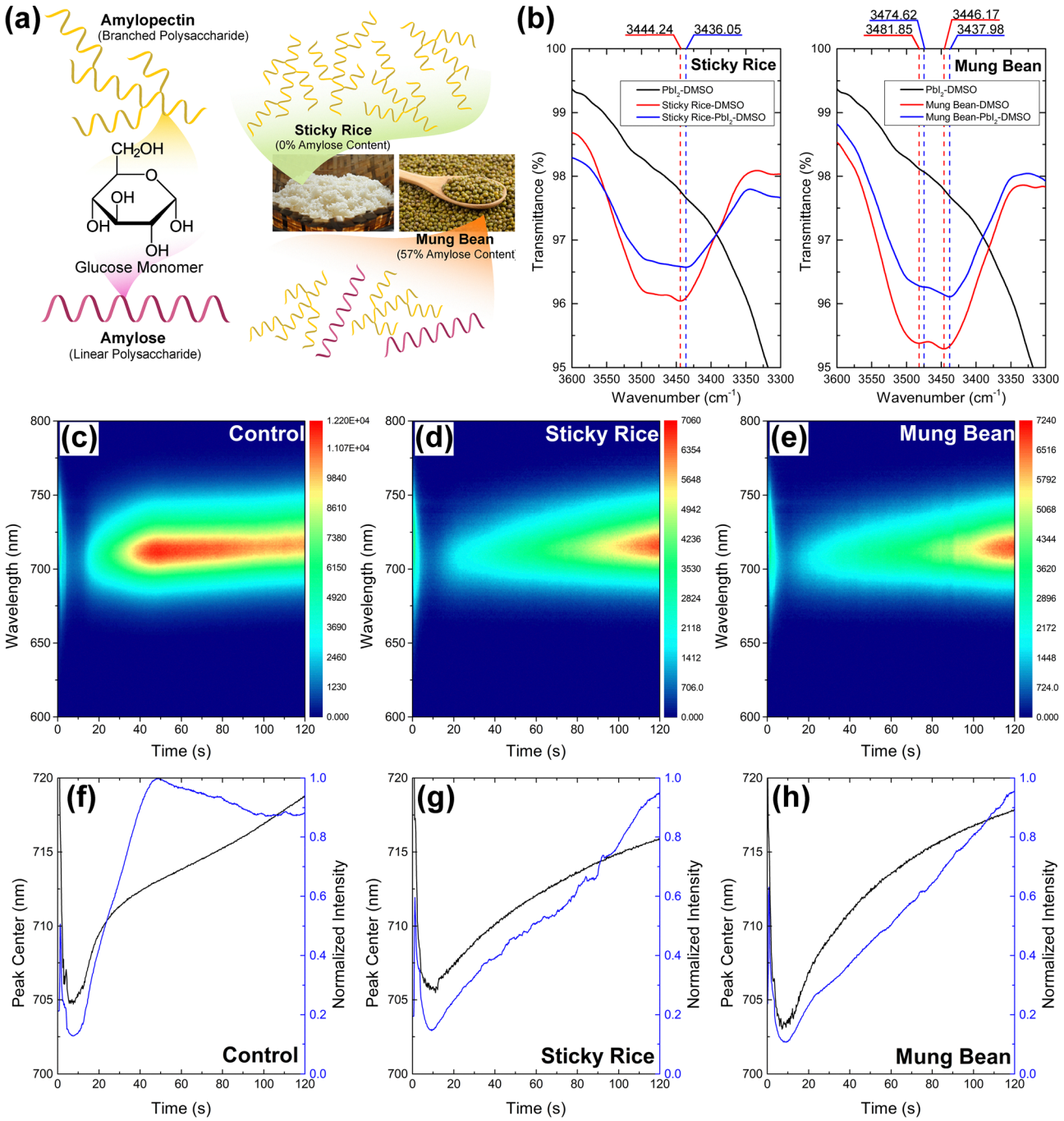

Fig. 1 (a) Schematic representation of the structures of amylose and amylopectin, including the amylose content in sticky rice and mung bean starches. (b) Expanded FTIR fingerprint region for –OH of PbI_2–DMSO (black), starch–DMSO (red), and starch–PbI_2–DMSO (blue) solutions. The dotted lines denoted corresponding peak positions, color-coded to match each spectrum. *In situ* PL of starch-treated precursors during spin-coating. PL heatmap with integrated PL peak center and normalized intensity evolution of control (c) and (f), sticky rice-modified (d) and (g), and mung bean-modified (e) and (h) perovskite precursors (quenching begins at 0 s).

the perovskite using the same process as that of the PSC fabrication before storage in a <10%RH desiccator. The carbon top-electrode was pressed on electron and hole only devices under the same conditions as those of perovskite solar cells. PCBM and Spiro-OMeTAD were deposited in a nitrogen-filled glovebox.

2.5 Characterization

A field emission scanning electron microscope (FE-SEM, JEOL JSM-7001F) was operated at 15 kV beam intensity to observe the morphology of the perovskite film. To study the phase formation of the perovskite in the 10–50° range of 2θ, a Rigaku Smartlab SE with a Cu Kα X-ray source was used. Steady-state photoluminescence (STPL) and time-resolved photoluminescence (TRPL) spectra were obtained with a 403 nm excitation laser using a spectrofluorometer from Horiba DeltraFlex and Pico Quant FluoTime 300. Fourier-transform infrared spectroscopy (FTIR, Thermo Scientific Nicolet iZ10) was performed on PbI_2 solution to observe starch–PbI_2 interactions. Formation of a starch barrier was observed using a transmission electron microscope (TEM, JEOL JEM-2100) at 160 kV beam intensity. An ultraviolet-visible spectrophotometer (UV-vis, Agilent 8453) was utilized to evaluate the amylose content of starch additives and the absorption range of perovskite films. Power conversion efficiency (PCE) and space-charge limiting current (SCLC), and maximum power point tracking (MPPT) with a perturb and observe (P&O) algorithm of the perovskite solar cells were measured using a Keithley 2400 source meter. PCE and P&O MPPT were measured on 0.12 cm^2 of the devices under AM1.5G illumination with 1000 W m^{-2} from a Xe short-arc lamp solar simulator (Enlitech SS-X50), calibrated using a silicon-based calibration cell (InfinityPV, CalCell). External quantum efficiency (EQE, Enlitech QE-R) was measured on the devices to determine the integrated current of the solar cells.

3. Results and discussion

To investigate how the polymeric structure of starch additives influences perovskite formation, we examine two types of starches: sticky rice starch (0 ± 2% amylose, predominantly branched-helical amylopectin) and mung bean starch (57 ± 2% amylose, a mixture of linear and branched helices), as shown in Fig. 1a and Fig. S2. The FTIR spectra in Fig. 1b and Fig. S3 show that sticky rice and mung bean dissolved in DMSO exhibit distinct single and two characteristic peaks, respectively. Upon incorporation of both the starch additives into the PbI_2–DMSO systems, the FTIR characteristic peaks of hydroxyl (–OH) stretching vibrations shift from 3444.24 cm^{-1} to 3436.05 cm^{-1} for sticky rice starch and from 3446.17 cm^{-1} to 3437.98 cm^{-1} for mung bean starch, associated with the –OH groups along branched amylopectin chains.[30] In the case of mung bean starch, an additional peak shift from 3481.85 cm^{-1} to 3474.62 cm^{-1} is also noticed, which likely corresponds to the stretching vibration of the –OH sites along the linear amylose chain.[31] These spectral shifts of the –OH stretching peaks imply coordination between the –OH sites along starch chains and the Pb^{2+} centers in PbI_2.[32] Such interactions explain the formation of starch–PbI_2–DMSO complexes within the perovskite precursor solutions, which could influence the subsequent perovskite crystallization process.[13]

In situ PL measurements were conducted during the spin coating process to examine the influence of these complexes on the perovskite formation process.[33] According to Fig. 1c and f, for the reference ink without starch additives, the perovskite starts forming at approximately 10 s after quenching, evident in a fast evolution of the PL signal both in terms of the emission peak position and integrated intensity. After 47.2 seconds, the PL intensity starts to decrease, which is attributed to the fast aggregation of perovskite clusters. This rapid nucleation and aggregation could result in the formation of poor-quality perovskite films.[34] The addition of sticky rice and mung bean starches to the perovskite precursors delays the evolution of PL signals, as shown in Fig. 1d, e and g, h, implying slower nucleation and aggregation of the perovskite clusters. This retarded growth of perovskite by the starches could lead to the formation of higher-quality perovskite films.[27,35]

The starch additives not only delay perovskite formation but also assist perovskite growth along their polymeric chains, which could enable the formation of high-quality absorbers in an ambient environment with high humidity. As shown in top-view scanning electron microscopy (SEM) images (Fig. 2a–c), both sticky rice and mung bean additives increase the average grain size of perovskite from 354 nm to 530 nm and 659 nm (Fig. S4), respectively. Moreover, the thickness of the perovskite films increased from 401 nm up to 535 nm and 567 nm by sticky rice and mung bean additives, respectively, as shown in the cross-sectional SEM images. An increase in the linear-amylose content in the starch additive not only enhances the grain size and thickness of the films but also minimizes vertical boundaries (Fig. 2c), thereby reducing defect sites in perovskite absorbers.[1] According to the XRD spectra in Fig. 2d, both starch additives significantly enhance the intensity of perovskite characteristic peaks in the {110} plane family, indicating that amylose and amylopectin template the growth of perovskite along the [110] direction. The mung bean starch with a higher linear-amylose content can serve as a molecular scaffold (Fig. 2e), more effectively than branched amylopectin, which leads to highly oriented perovskite along the [110] direction (Fig. S5). This enhancement of preferred orientation can promote carrier transportation across the perovskite film thickness.[36]

Further investigation using a transmission electron microscope (TEM) reveals nanometer-thick starch layers surrounding perovskite grains, shown in Fig. 3a, which possibly are networks of starch induced by heat during fabrication. These starch layers are believed to passivate accumulated defects at grain boundaries.[37] To confirm this hypothesis, X-ray photoelectron spectroscopy (XPS) was performed on perovskite films with and without the additives to investigate the interaction between the starch additives and the perovskite. As shown in Fig. S6, there are shifts in the Pb 4f and I 3d core levels in the

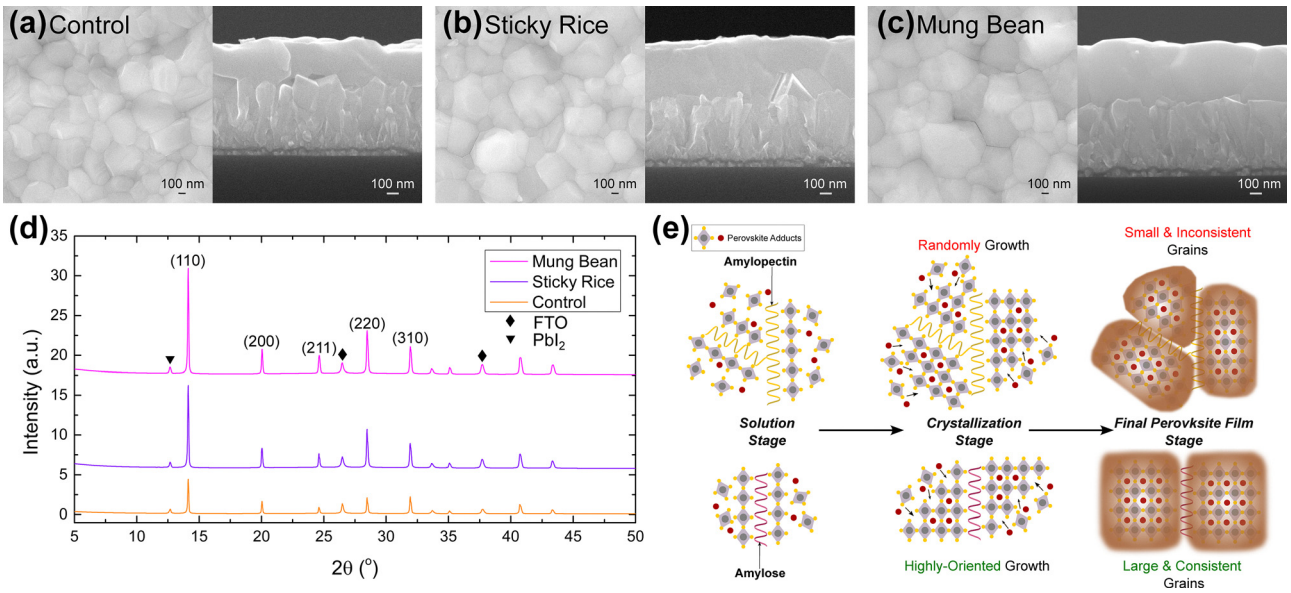

Fig. 2 Top-view and cross-sectional SEM images of (a) control, (b) sticky rice-modified, and (c) mung bean-modified perovskite films. (d) The XRD spectra of perovskite films on FTO substrates, fabricated from perovskite precursors without and with starch additives. (e) Schematic of perovskite growth kinetics assisted by amylopectin and amylose.

case of perovskite with the incorporation of the starch additives, which are attributed to the chemical interactions between the hydroxyl groups along starch chains and defect sites within the perovskite films (*i.e.*, undercoordinated Pb^{2+} and iodine vacancies).[38,39] These interactions highlight the ability of the starch additives to passivate defects, improving the optoelectronic quality of perovskite absorbers fabricated under ambient conditions.

To investigate the influence of improved perovskite film morphology by the starch additives on the optoelectronic quality, we performed photoluminescence (PL) spectroscopy and space-charge-limited current (SCLC) measurements.[37] As shown in Fig. 3b, the high-linear amylose starch modified-perovskite film (mung bean) radiatively luminesces the strongest from the steady-state photoluminescence (STPL) measurement. Additionally, mung bean-modified perovskite films exhibit longer average charge carrier lifetimes of 346.50 ns, compared to 226.59 ns for the control and 276.50 ns for the sticky rice-modified films, as fitted from the time-resolved photoluminescence (TRPL) spectra (Fig. 3c) by bi-exponential decay. These observed improvements in STPL and carrier lifetimes signify a superior reduction in non-radiative recombination by linear amylose, likely due to more effective defect passivation.[27,40] Space-charge-limited current (SCLC) measurement (Fig. 3d and e) was further performed to quantify electron ($n_{t,e}$) and hole trap ($n_{t,h}$) densities in perovskite films using eqn (1).

$$n_t = \frac{2\varepsilon\varepsilon_0}{qd^2} V_{TFL}, \quad (1)$$

where ε_0, ε, q, d, and V_{TFL} are vacuum permittivity, relative permittivity (62.23 for CsFA-based perovskite),[41] elementary charge, perovskite film thickness, and trap-filled limit voltage, respectively. Table 1 shows that sticky rice and mung bean additives dramatically reduce the number of electron trap density from 8.30×10^{15} cm^{-3} to 4.72×10^{15} and 4.67×10^{15} cm^{-3}, respectively. In the same way, hole trap density is also decreased from 3.02×10^{15} cm^{-3} to 1.71×10^{15} and 1.53×10^{15} cm^{-3} in the case of sticky rice and mung bean additives, respectively. These

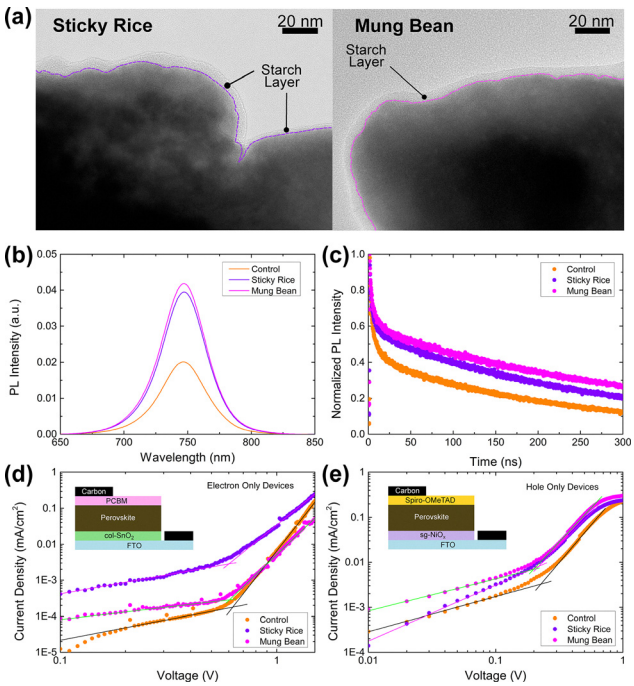

Fig. 3 (a) TEM images of the perovskite grains covered by starch layers. The (b) STPL and (c) TRPL spectra of the perovskite film fabricated under ambient conditions on FTO substrates without and with sticky rice and mung bean additives. The dark *J*–*V* curve of (d) electron-only and (e) hole-only devices with V_{TFL} evaluated from interceptions.

Table 1 Calculated electron and hole trap density from SCLC measurement

Conditions	Electron-only device		Hole-only device	
	V_{TFL}	$n_{t,e}$ (cm^{-3})	V_{TFL}	$n_{t,h}$ (cm^{-3})
Control	0.624	8.30×10^{15}	0.227	3.02×10^{15}
Sticky rice	0.597	4.72×10^{15}	0.217	1.71×10^{15}
Mung bean	0.605	4.67×10^{15}	0.198	1.53×10^{15}

results confirm the hypothesis that linear amylose most effectively passivates perovskite defects, which could be beneficial for device performance improvement compared to starch additives with branched amylopectin.

We explore the impact of starch additives on the performance of all-solution-processed PSCs with an FTO/col–SnO_2/ambient condition-fabricated perovskite/spiro–OMeTAD/carbon architecture. Starch additives help improve reproducibility, observed by narrower distributions of power conversion efficiency (PCE), shown in Fig. 4a. Additionally, Fig. 4b shows that the best performance of ambient fabricated perovskite with carbon electrode PSCs increases from 14.05% up to 14.99% (sticky rice) and 16.17% (mung bean). This enhancement in performance is attributed to increases in the open-circuit voltage (V_{oc}), fill-factor (FF), and short-circuit current density (J_{sc}), as summarized in Fig. S7 and Table S1. The average V_{oc} of starch-modified PSCs improves from 1.013 V to 1.033 V (sticky rice) and 1.035 V (mung bean). Additionally, the average FF of sticky rice- and mung bean-modified PSCs also increases from 56.14% up to 63.89 and 63.93%, respectively. These improvements are consistent with the reduction of non-radiative recombination, due to defect suppression in perovskite layers.[1] Furthermore, improvement of average J_{sc} from 18.42 mA cm^{-2} to 19.91 and 19.92 mA cm^{-2} by sticky rice and mung bean modification, respectively, agrees with the EQE results, shown in Fig. 4c. This is attributed to stronger light absorption in the visible range (Fig. S8) by the thicker perovskite absorber and enhanced carrier mobility from significant suppression of trap densities.[42]

To investigate the effect of starch additives on the durability of perovskites, ambient-fabricated films are aged under extreme storage conditions, including moisture (25–35 °C/60–80%RH, ISOS-D-1) and moisture-heat (85 °C/60–80%RH, ISOS-D-2).[43]

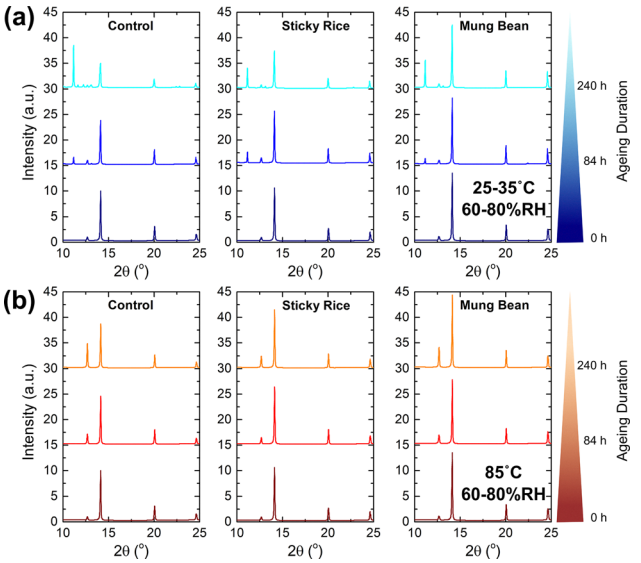

Fig. 5 Evolution of XRD profiles of the perovskite films without and with the starch additives aging under (a) moisture (25–35 °C/60–80%RH) and (b) moisture-heat (85 °C/60–80%RH) conditions for 240 hours.

The XRD spectra in Fig. 5a and b show that starch-modified perovskite films maintain higher intensity of the perovskite characteristic peaks and low intensity of non-perovskite phases (*i.e.*, PbI_2) after 240 hours of testing, compared to the control film. The enhanced stability stems from high-quality perovskite films with enlarged grains, increased compactness, and reduced defect density, resulting from the incorporation of starch additives.[44] A comparison of the XRD results from both starch additives reveals that mung bean-modified perovskite exhibits superior stabilities, as evidenced by the slower evolution of the PbI_2/(110) and (110)/$(110)_{initial}$ peak ratios in Fig. S9. This is attributed to linear-amylose in mung bean starch, which promotes film morphology and tightly wraps perovskite grains, more effectively passivating accumulated defects.

To assess the operational stability of starch-modified PSCs, we track the performance evolution of carbon-based PSCs without encapsulation at the maximum-power point using a perturb and observe (P&O) algorithm under 50–60% RH/25 °C/1 Sun-AM1.5G (ISOS-L-1).[43] Additionally, we develop a model (see

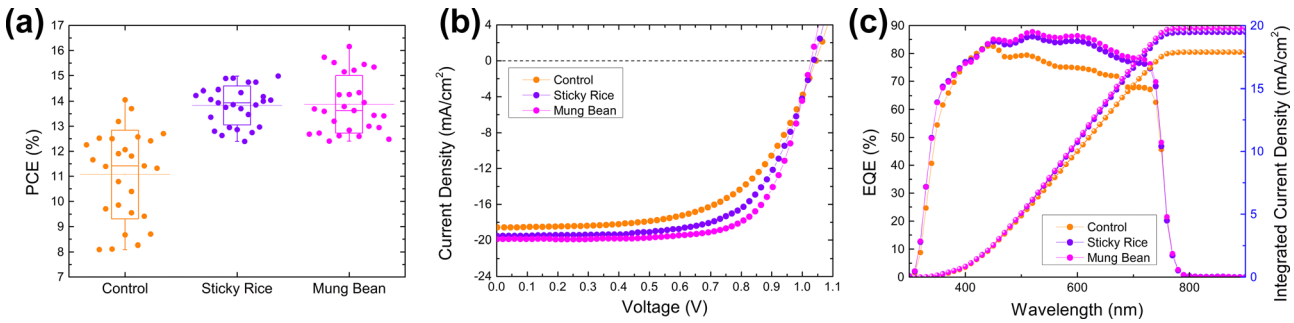

Fig. 4 (a) Performance statistics from 27 devices and (b) the best *J*–*V* curves in the reverse-scanned direction of PSCs with FTO/col–SnO_2/perovskite/spiro–OMeTAD/carbon structure without and with different starch additives. (c) The EQE spectra of representative PSCs without and with sticky rice and mung bean additives.

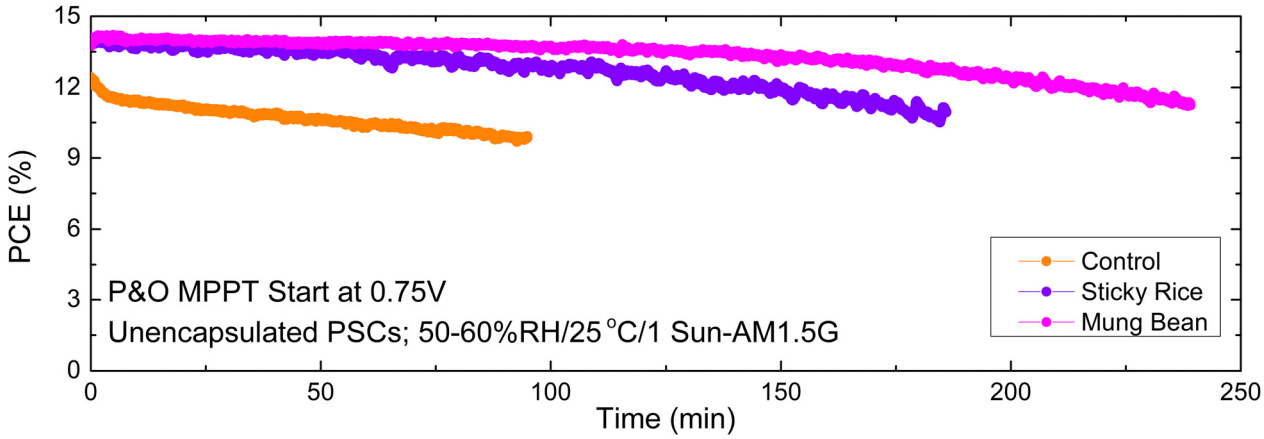

Fig. 6 Normalized performance evolution of unencapsulated perovskite solar cells without and with different starch additives during P&O MPPT under 50–60%RH/25 °C/1 Sun-AM1.5G (ISOS-L-1).

SI Note S1) for fitting the ageing curves to determine their lifetimes and better understand the degradation behavior of each device. As illustrated in Fig. 6 and Fig. S10, the devices with starch-modified perovskite absorbers show a very different ageing dynamics compared to the control device. The performance evolution of the control PSC exhibits a bi-exponential decay with initial burn-in, which is likely from ion-migration in the defective perovskite absorber.[45] In contrast, the starch-modified devices do not have burn-in but only slight linear degradation followed by a catastrophic failure, as shown in Fig. S11. This is likely caused by the moisture ingress over time. With proper packaging, starch-modified PSCs could potentially achieve longer operational lifetimes;[46] however, this aspect is beyond the scope of this study. On comparing the lifetimes of both starch-modified devices, shown in Table S2, it can be observed that the mung bean-treated PSC has the highest lifetime, corresponding to higher-quality film morphology (Fig. 2a–c) and superior defect passivation (Fig. 3d and e). This result highlights the importance of linear amylose in templating the growth of highly oriented perovskites together with grain wrapping, which is advantageous to achieve fully solution-processed PSCs fabricated under ambient conditions with enhanced performance and stability.

4. Conclusion

In summary, this work highlights the critical role of a polysaccharide molecular structure in templating perovskite crystallization, defect passivation, and device performance under high-humidity conditions (50% RH). We show that mung bean starch (57% linear amylose) facilitates the growth of highly oriented and larger perovskite grains with fewer vertical grain boundaries compared to sticky rice starch (100% branched amylopectin). The linear amylose chains interact chemically and physically with the perovskite defects, reduce trap densities by half, and suppress non-radiative recombination. These effects translate to a significant improvement in all-solution-processed carbon-based PSCs under high humidity conditions, boosting the efficiency from 14.05% to 16.17%. Remarkably, the linear-amylose-modified perovskite also mitigates burn-in degradation and doubles the operational lifetime of unencapsulated devices under ISOS-L-1 testing under 50–60%RH conditions. Ultimately, this study shows that selecting natural materials with suitable structures is key to promoting perovskite growth and passivating defects, which enable low-cost and sustainable PSC fabrication under ambient conditions.

Author contributions

C. H.: methodology, investigation, data curation, formal analysis, and writing – original draft. R. M.: formal analysis and writing – review and editing. Y. L.: *in situ* PL measurement and analysis. N. R.: equipment support for STPL, TRPL, XRD, and EQE measurements. E. U.: validation, resources, and writing – review and editing. R. C.: conceptualization, methodology, investigation, validation, supervision, formal analysis, writing – review and editing, funding acquisition, resources, and project administration.

Conflicts of interest

There are no conflicts to declare.

Data availability

The authors affirm that all data supporting the findings of this study are contained within the main article and the accompanying supplementary information (SI). Supplementary information: Performance parameters of ambient-fabricated perovskite layer with different starch additive concentration, starch additive characterization, FTIR spectra, perovskite grain size histogram, evolution of XRD peak ratios, XPS spectra of perovskite films, *JV* curves and performance statistic of ambient-fabricated PSCs, UV-vis spectra of perovskite films, evolution of PbI_2/(110) and (110)/(110) initial XRD peak ratios during aging, MPPT

curves, fitting model for MPPT curves. See DOI: https://doi.org/10.1039/d5qm00493d.

Acknowledgements

This research was funded by the 90th Anniversary of Chulalongkorn University Scholarship under the Ratchadapisek Somphot Endowment Fund (GCUGR1125671123D). C. H. gratefully acknowledges the Development and Promotion of Science and Technology Talents Project (DPST) for personal financial support. Additionally, C. H. gratefully thanks Nathampapop Jobsri and Chattarin Muensuksaeng for their valuable suggestions on manuscript improvement.

References

1 M. Hu, Y. Zhu, Z. Zhou, M. Hao, C. Harnmanasvate, J. Waiyawat, Y. Wang, J. Lu, Q. An, X. Li and T. Zhang, Post-Treatment of Metal Halide Perovskites: From Morphology Control, Defect Passivation to Band Alignment and Construction of Heterostructures, *Adv. Energy Mater.*, 2023, **2301888**, 1–26.

2 S. Wang, L. Tan, J. Zhou, M. Li, X. Zhao, H. Li, W. Tress, L. Ding, M. Graetzel and C. Yi, Over 24% Efficient MA-free $Cs_xFA_{1-x}PbX_3$ perovskite solar cells, *Joule*, 2022, **6**, 1344–1356.

3 J. J. Yoo, G. Seo, M. R. Chua, T. G. Park, Y. Lu, F. Rotermund, Y. K. Kim, C. S. Moon, N. J. Jeon, J. P. Correa-Baena, V. Bulović, S. S. Shin, M. G. Bawendi and J. Seo, Efficient Perovskite Solar Cells via Improved Carrier management, *Nature*, 2021, **590**, 587–593.

4 H. Su, J. Xiao, Q. Li, C. Peng, X. Zhang, C. Mao, Q. Yao, Y. Lu, Z. Ku, J. Zhong, W. Li, Y. Peng, F. Huang and Y. bing Cheng, Carbon Film Electrode Based Square-Centimeter Scale Planar Perovskite Solar Cells Exceeding 17% Efficiency, *Mater. Sci. Semicond. Process.*, 2020, **107**, 104809.

5 K. Zhang, Z. Wang, G. Wang, J. Wang, Y. Li, W. Qian, S. Zheng, S. Xiao and S. Yang, A Prenucleation Strategy for Ambient Fabrication of Perovskite Solar Cells with High Device Performance Uniformity, *Nat. Commun.*, 2020, **11**, 1–11.

6 Y. Zhao, I. Yavuz, M. Wang, M. H. Weber, M. Xu, J. H. Lee, S. Tan, T. Huang, D. Meng, R. Wang, J. Xue, S. J. Lee, S. H. Bae, A. Zhang, S. G. Choi, Y. Yin, J. Liu, T. H. Han, Y. Shi, H. Ma, W. Yang, Q. Xing, Y. Zhou, P. Shi, S. Wang, E. Zhang, J. Bian, X. Pan, N. G. Park, J. W. Lee and Y. Yang, Suppressing Ion Migration in Metal Halide Perovskite via Interstitial Doping with A Trace Amount of Multivalent Cations, *Nat. Mater.*, 2022, **21**, 1396–1402.

7 H. Li, T. Bu, J. Li, Z. Lin, J. Pan, Q. Li, X. L. Zhang, Z. Ku, Y. B. Cheng and F. Huang, Ink Engineering for Blade Coating FA-Dominated Perovskites in Ambient Air for Efficient Solar Cells and Modules, *ACS Appl. Mater. Interfaces*, 2021, **13**, 18724–18732.

8 K. S. Lim, D. K. Lee, J. W. Lee and N. G. Park, 17% Efficient Perovskite Solar Mini-Module: Via Hexamethylphosphoramide (HMPA)-Adduct-based Large-Area D-bar Coating, *J. Mater. Chem. A*, 2020, **8**, 9345–9354.

9 Y. Huang, W. Zhang, Y. Xiong, Z. Yi, C. Huang, Q. Jiang, A. Basit, G. Shen, Y. Luo, X. Li and J. Yang, Recent Advancements in Ambient-Air Fabrication of Perovskite Solar Cells, *Exploration*, 2025, 20240121, DOI: 10.1002/EXP.20240121.

10 K. Mo, X. Zhu, M. Yang, Z. Xue, S. Li, Y. Yang, S. Cheng, H. Li, Q. Lin and Z. Wang, Minimizing DMSO Residues in Perovskite Films for Efficient and Long-Term Stable Solar Cells, *Adv. Energy Mater.*, 2025, **2404538**, 1–7.

11 K. Jung, K. Oh, D. H. Kim, J. W. Choi, K. C. Kim and M. J. Lee, Ambient-Air Fabrication of Stable Mixed Cation Perovskite Planar Solar Cells with Efficiencies Exceeding 22% Using A Synergistic Mixed Antisolvent with Complementary Properties, *Nano Energy*, 2021, **89**, 106387.

12 L. Yan, H. Huang, P. Cui, S. Du, Z. Lan, Y. Yang, S. Qu, X. Wang, Q. Zhang, B. Liu, X. Yue, X. Zhao, Y. Li, H. Li, J. Ji and M. Li, Fabrication of Perovskite Solar Cells in Ambient Air by Blocking Perovskite Hydration with Guanabenz Acetate Salt, *Nat. Energy*, 2023, **8**, 1158–1167.

13 D. Bi, C. Yi, J. Luo, J. D. Décoppet, F. Zhang, S. M. Zakeeruddin, X. Li, A. Hagfeldt and M. Grätzel, Polymer-Templated Nucleation and Crystal Growth of Perovskite Films for Solar Cells with Efficiency Greater Than 21%, *Nat. Energy*, 2016, **1**, 1–5.

14 T. H. Han, J. W. Lee, C. Choi, S. Tan, C. Lee, Y. Zhao, Z. Dai, N. De Marco, S. J. Lee, S. H. Bae, Y. Yuan, H. M. Lee, Y. Huang and Y. Yang, Perovskite-Polymer Composite Cross-Linker Approach for Highly-Stable and Efficient Perovskite Solar Cells, *Nat. Commun.*, 2019, **10**, 1–10.

15 H. Guo, G. W. Yoon, Z. J. Li, Y. Yun, S. Lee, Y. H. Seo, N. J. Jeon, G. S. Han and H. S. Jung, Enabling Photostable Perovskite Solar Cells via Sustainable Operando Defect-Passivation Strategy, *Adv. Energy Mater.*, 2024, **14**, 1–10.

16 S. Wang, X. Y. Gong, M. X. Li, M. H. Li and J. S. Hu, Polymers for Perovskite Solar Cells, *JACS Au*, 2024, **4**, 3400–3412, DOI: 10.1021/jacsau.4c00615.

17 N. Forfora, I. Azuaje, T. Kanipe, J. A. Gonzalez, M. Lendewig, I. Urdaneta, R. Venditti, R. Gonzalez and D. Argyropoulos, Are Starch-Based Materials More Eco-Friendly Than Fossil-Based? A Critical Assessment, *Clean. Environ. Systems*, 2024, **13**, 100177.

18 P. Usubharatana and H. Phungrassami, Carbon Footprint of Cassava Starch Production in North-Eastern Thailand, *Procedia CIRP*, 2015, **29**, 462–467.

19 R. Anthony, M. A. Sharara, T. M. Runge and R. P. Anex, Life Cycle Comparison of Petroleum- and Bio-based Paper Binder from Distillers Grains (DG), *Ind. Crops Prod.*, 2017, **96**, 1–7.

20 A. Islam, K. Usman, Z. Haider, M. F. Alam, A. Nawaz and P. Sonar, Biomass-Derived Materials for Interface Engineering in Organic/Perovskite Photovoltaic and Light-Emitting

Devices, *Adv. Mater. Technol.*, 2023, **8**, 1–41, DOI: **10.1002/admt.202201390**.

21 J. Han, Y. Tian and I. Jeon, Natural and Nature-Inspired Biomaterial Additives for Metal Halide Perovskite Optoelectronics, *Adv. Mater.*, 2024, **2410327**, 1–24, DOI: **10.1002/adma.202410327**.

22 Z. Günkaya and M. Banar, An Environmental Comparison of Biocomposite Film Based on Orange Peel-Derived Pectin Jelly-Corn Starch and LDPE Film: LCA and Biodegradability, *Int. J. Life Cycle Assess.*, 2016, **21**, 465–475.

23 L. Zuo, H. Guo, D. W. DeQuilettes, S. Jariwala, N. De Marco, S. Dong, R. DeBlock, D. S. Ginger, B. Dunn, M. Wang and Y. Yang, Polymer-Modified Halide Perovskite Films for Efficient and Stable Planar Heterojunction Solar Cells, *Sci. Adv.*, 2017, **3**, 1–12.

24 D. Seung, Amylose in Starch: Towards An Understanding of Biosynthesis, Structure and Function, *New Phytol.*, 2020, **228**, 1490–1504.

25 H. Zheng, G. Liu, W. Wu, H. Xu and X. Pan, Highly Efficient and Stable Perovskite Solar Cells with Strong Hydrophobic Barrier via Introducing Poly(vinylidene fluoride) Additive, *J. Energy Chem.*, 2021, **57**, 593–600.

26 C. Hernandez-Jaimes, C. Lobato-Calleros, E. Sosa, L. A. Bello-Pérez, E. J. Vernon-Carter and J. Alvarez-Ramirez, Electrochemical Characterization of Gelatinized Starch Dispersions: Voltammetry and Electrochemical Impedance Spectroscopy on Platinum Surface, *Carbohydr. Polym.*, 2015, **124**, 8–16.

27 C. Harnmanasvate, R. Chanajaree, N. Rujisamphan, Y. Rong and R. Cheacharoen, Ambient Gas-Quenching Fabrication of MA-Free Perovskite Solar Cells Enabled by an Eco-Friendly Urea Additive, *ACS Appl. Energy Mater.*, 2023, **6**, 10665–10673.

28 P. Chen, J. Hu, M. Yu, P. Li, R. Su, Z. Wang, L. Zhao, S. Li, Y. Yang, Y. Zhang, Q. Li, D. Luo, Q. Gong, E. H. Sargent, R. Zhu and Z. H. Lu, Refining Perovskite Heterojunctions for Effective Light-Emitting Solar Cells, *Adv. Mater.*, 2023, **35**, 1–12.

29 R. Cheacharoen, C. C. Boyd, G. F. Burkhard, T. Leijtens, J. A. Raiford, K. A. Bush, S. F. Bent and M. D. McGehee, Encapsulating Perovskite Solar Cells to Withstand Damp Heat and Thermal Cycling, *Sustainable Energy Fuels*, 2018, **2**, 2398–2406.

30 I. Rashid, M. H. Al Omari, S. A. Leharne, B. Z. Chowdhry and A. Badwan, Starch Gelatinization Using Sodium Silicate: FTIR, DSC, XRPD, and NMR Studies, *Starch/Staerke*, 2012, **64**, 713–728.

31 P. Jha, Functional Properties of Starch-Chitosan Blend Bionanocomposite Films for Food Packaging: The Influence of Amylose-Amylopectin Ratios, *J. Food Sci. Technol.*, 2021, **58**, 3368–3378.

32 B. Li, D. Binks, G. Cao and J. Tian, Engineering Halide Perovskite Crystals through Precursor Chemistry, *Small*, 2019, **15**, 1–24.

33 T. Huang, S. Tan, S. Nuryyeva, I. Yavuz, F. Babbe, Y. Zhao, M. Abdelsamie, M. H. Weber, R. Wang, K. N. Houk, C. M. Sutter-Fella and Y. Yang, Performance-Limiting Formation Dynamics in Mixed-Halide perovskites, *Sci. Adv.*, 2021, **7**, 1–10.

34 H. Min, J. Chang, Y. Tong, J. Wang, F. Zhang, Z. Feng, X. Bi, N. Chen, Z. Kuang, S. Wang, L. Yuan, H. Shi, N. Zhao, D. Qian, S. Xu, L. Zhu, N. Wang, W. Huang and J. Wang, Additive Treatment Yields High-Performance Lead-Free Perovskite Light-Emitting Diodes, *Nat. Photonics*, 2023, **17**, 755–760.

35 C. Pereyra, H. Xie and M. Lira-Cantu, Additive Engineering for Stable Halide Perovskite Solar Cells, *J. Energy Chem.*, 2021, **60**, 599–634.

36 Y. Zhao, Y. Tan, L. Wan, L. Lou and Z. S. Wang, Tryptaminium Iodide as an Additive of Isopropanol Green Antisolvent for Efficient and Stable Perovskite Solar Cells, *ACS Appl. Energy Mater.*, 2022, **5**, 9520–9529.

37 Y. Bai, Y. Lin, L. Ren, X. Shi, E. Strounina, Y. Deng, Q. Wang, Y. Fang, X. Zheng, Y. Lin, Z. G. Chen, Y. Du, L. Wang and J. Huang, Oligomeric Silica-Wrapped Perovskites Enable Synchronous Defect Passivation and Grain Stabilization for Efficient and Stable Perovskite Photovoltaics, *ACS Energy Lett.*, 2019, **4**, 1231–1240.

38 Z. Guo, S. Zhao, N. Shibayama, A. Kumar Jena, I. Takei and T. Miyasaka, A Universal Method of Perovskite Surface Passivation for $CsPbX_3$ Solar Cells with VOC over 90% of the S-Q limit, *Adv. Funct. Mater.*, 2022, **32**, 1–9.

39 H. Huang, Z. Li, Z. Chen, D. Li, H. Shi, K. Zhu, C. Wang, Z. Lu, S. Huang and D. Chi, Interfacial Modification Engineering for Efficient and Stable MA-Free Wide-Bandgap Perovskite Solar Cells by Grain Regrowth, *Mater. Chem. Front.*, 2024, **8**, 3017–3027.

40 B. Gogoi, A. Yerramilli, K. M. Luboowa, S. M. Shin and T. L. Alford, Understanding The Crystallization of Triple-Cation Perovskites Assisted by Mixed Antisolvents for Improved Solar Cell Device Performance, *J. Mater. Sci.: Mater. Electron.*, 2022, **33**, 4415–4425.

41 D. Yang, R. Yang, K. Wang, C. Wu, X. Zhu, J. Feng, X. Ren, G. Fang, S. Priya and S. (Frank) Liu, High efficiency planar-type perovskite solar cells with negligible hysteresis using EDTA-complexed SnO_2, *Nat. Commun.*, 2018, **9**, 1–11, DOI: **10.1038/s41467-018-05760-x**.

42 Y. Sun, S. Yang, Z. Pang, Y. Quan, R. Song, Y. Chen, W. Qi, Y. Gao, F. Wang, X. Zhang, Y. Sun, J. Yang, L. Yang and F. Rosei, Preferred Film Orientation to Achieve Stable and Efficient Sn-Pb Binary Perovskite Solar Cells, *ACS Appl. Mater. Interfaces*, 2021, **13**, 10822–10836, DOI: **10.1021/acsami.0c19014**.

43 M. V. Khenkin, E. A. Katz, A. Abate, G. Bardizza, J. J. Berry, C. Brabec, F. Brunetti, V. Bulović, Q. Burlingame, A. Di Carlo, R. Cheacharoen, Y. B. Cheng, A. Colsmann, S. Cros, K. Domanski, M. Dusza, C. J. Fell, S. R. Forrest, Y. Galagan, D. Di Girolamo, M. Grätzel, A. Hagfeldt, E. von Hauff, H. Hoppe, J. Kettle, H. Köbler, M. S. Leite, S. (Frank) Liu, Y. L. Loo, J. M. Luther, C. Q. Ma, M. Madsen, M. Manceau, M. Matheron, M. McGehee, R. Meitzner, M. K. Nazeeruddin, A. F. Nogueira, Ç. Odabaşı, A. Osherov, N. G. Park,

M. O. Reese, F. De Rossi, M. Saliba, U. S. Schubert, H. J. Snaith, S. D. Stranks, W. Tress, P. A. Troshin, V. Turkovic, S. Veenstra, I. Visoly-Fisher, A. Walsh, T. Watson, H. Xie, R. Yıldırım, S. M. Zakeeruddin, K. Zhu and M. Lira-Cantu, Consensus Statement for Stability Assessment and Reporting for Perovskite Photovoltaics Based on ISOS Procedures, *Nat. Energy*, 2020, **5**, 35–49.

44 J. W. Lee, S. H. Bae, Y. T. Hsieh, N. De Marco, M. Wang, P. Sun and Y. Yang, A Bifunctional Lewis Base Additive for Microscopic Homogeneity in Perovskite Solar Cells, *Chem*, 2017, **3**, 290–302.

45 C. Ding, L. Yin, J. Wang, V. Larini, L. Zhang, R. Huang, M. Nyman, L. Zhao, C. Zhao, W. Li, Q. Luo, Y. Shen, R. Österbacka, G. Grancini and C. Q. Ma, Boosting Perovskite Solar Cells Efficiency and Stability: Interfacial Passivation of Crosslinked Fullerene Eliminates the ''Burn-in'' Decay, *Adv. Mater.*, 2023, **35**, 1–10.

46 S. Alam, M. M. Islam, S. Chowdhury, R. Meitzner, C. Kästner, U. S. Schubert and H. Hoppe, Disentanglement of Degradation Mechanisms by Analyzing Aging Dynamics of Environmentally Friendly Processed Polymer Solar Cells, *Energy Technol.*, 2020, **8**, 19–23.